

## CONVECTIVE HEAT TRANSFER ENHANCEMENT VIA ELECTRICALLY DRIVEN VORTICES IN AN MHD DUCT FLOW

**Ahmad H. A. HAMID<sup>1,2,\*</sup>, Wisam K. HUSSAM<sup>1</sup> and Gregory J. SHEARD<sup>1,†</sup>**

<sup>1</sup> The Sheard Lab, Department of Mechanical and Aerospace Engineering, Monash University, Victoria 3800, AUSTRALIA

† E-mail address: Greg.Sheard@monash.edu

<sup>2</sup> Faculty of Mechanical Engineering, Universiti Teknologi MARA, 40450 Selangor, MALAYSIA

\*Corresponding author, E-mail address: hussein@salam.uitm.edu.my

### ABSTRACT

The design of vortex promoters in a heated wall duct is often limited by the considerations of practicality, especially in complex systems such as a fusion blanket. In the present study, a high-order spectral-element method is employed to solve the quasi-two-dimensional magnetohydrodynamic duct flow and heat transport. Electric currents from electrodes embedded in the duct walls are used to enhance instability in the cylinder wake, and thus the convective heat transfer from a duct wall is investigated. The hot and cold walls are parallel to the magnetic field, which is imposed in the direction parallel to the cylinder axis. The strength of the magnetic field, which is quantified by the friction parameter  $H$ , is varied between 200 and 2500, to explore its influences on the convective heat transport phenomenon. This investigation builds on a recommendation from previous work dedicated to understanding of the flow stability in a similar configuration. The results indicate that the imposed magnetic field strength and current injection significantly alters the dynamics behaviour of the wake behind a cylinder, and that the convective heat transfer improves by almost 50% with negligible additional pressure loss.

### NOMENCLATURE

$\zeta$	vorticity
$\eta$	efficiency index
$\rho$	density
$\sigma$	electrical conductivity
$\theta$	temperature
$\tau$	pulse width
$\mu$	dynamic viscosity
$\psi_0$	electrical potential
$\omega_f$	current frequency
$a$	duct depth (out of plane)
$B$	uniform magnetic field strength
$D$	current pulse duty cycle
$H$	Hartmann friction parameter
$HR$	heat transfer enhancement ratio
$I$	current amplitude
$\mathbf{j}$	current density
$L$	characteristic length
$Nu$	Nusselt number
$n$	number of Hartmann walls
$PR$	pressure penalty ratio
$Pe$	Peclet number

$Pr$	Prandtl number
$p$	pressure
$Re_L$	Reynolds number
$t$	time
$\mathbf{u}$	velocity
$U_0$	peak fluid velocity at duct inlet

### INTRODUCTION

In magnetohydrodynamic (MHD) duct flows, an electrically conducting fluid flows under the influence of magnetic field. The interaction between induced electric currents and the applied magnetic field results in an electromagnetic Lorentz force, which in turn gives a damping effect to the flows (Sommeria and Moreau 1982). The study of MHD flow in ducts in the presence of a transverse magnetic field is important because of its practical applications in MHD generators, pumps, metallurgical processing and magnetic confinement fusion reactors.

In practical situations like in coolant blankets of fusion reactors, the fundamental physics of MHD bears critical consequences. The coolant flow, which is used to evacuate the heat generated by the nuclear fusion, tends to two-dimensionality under a strong magnetic field (Douset and Pothérat 2008). It has been shown previously that MHD effects serve to reduce the thermal-hydraulic performance by greatly reducing the heat transfer coefficient and increasing the pressure drop through laminarization of the flow (Hussam and Sheard 2013). The cooling process can be assisted by mixing of the flow via turbulence or vortical structures. The vortex motion induces significant velocity component in transverse direction and thus improving convective heat transport in this direction.

The heat transfer can be further improved by modifying the kinematics of these wake vortices via an active or passive excitation. Hussam, Thompson and Sheard (2012) reported that the optimum perturbations leading to Kármán vortex shedding are localized in the near-wake region around the cylinder, which can be accomplished by a geometric configuration alteration (in passive mode) and by a cylinder oscillation (in active mode). It has been found that increasing oscillation amplitude leads to a higher convective heat transfer from a hot wall (Beskok, Raisee, Celik, Yagiz and Cheraghi 2012), through the gains become more modest at larger amplitudes (Hussam, Thompson and Sheard 2012).

In non-MHD cases, a remarkable heat transfer enhancement associated with active excitation has been reported (Fu and Tong 2004, Celik, Akdag, Gunes and Beskok 2008, Celik, Raisee and Beskok 2010, Beskok *et*

al. 2012). However, studies relevant to duct heat transfer enhancement in an MHD flows are rather scarce (Hussam *et al.* 2012). Furthermore, employing a mechanical actuator for such turbulizers in a duct faces significant technical obstacles to a practical implementation. Alternatively, one can take advantage of the MHD flow characteristics, i.e. the presence of an imposed magnetic field in an electrically conducting flow, to intensify vortical structures by means of electric current injection, either from an electrode mounted flush with one of the Hartmann walls, or from the conducting cylinder. The design and implementation of such a system would be more practical and simpler as compared to a mechanically actuated turbulence promoter system. This idea has been already used by Pothérat and Klein (2014) to generate vortices parallel to the imposed magnetic field, but not yet in a duct arrangement with side-wall heating.

In the present study, the coupled effects of the induced Lorentz force due to the imposed-current and induced-current on the heat transfer, pressure drop and efficiency enhancement for the cylinder wake flows are investigated. We are particularly interested in a flow with Reynolds number  $Re = 1500$  in a duct with a blockage ratio  $\beta = 0.2$ . Owing to the fact that there is a limited number of studies on an actively excited cylinder wake vortices in an MHD duct flow in the literature, the present investigation is anticipated to furnish valuable information for the design of efficient heat transport systems in high-magnetic-field applications.

## NUMERICAL IMPLEMENTATION

### Governing Equations

In the current investigation a flow of electrically conducting fluid passing over a circular cylinder placed in the center of the duct is considered (as depicted in Fig. 1). The bottom wall of the duct is uniformly heated. A constant uniform magnetic field is imposed in the axial direction. The wake flow is modified by means of current injection through the cylinder. A quasi-two-dimensional (quasi-2D) model for MHD duct flow (Sommeria *et al.* 1982) is employed. Generally this model, called thereafter SM82 model, is applicable for MHD duct flows under the influence of a strong transverse magnetic field. Under this condition, the core flow exhibit uniform velocity (as depicted in Fig. 2).

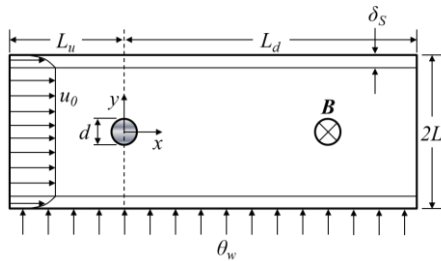


**Figure 1:** Schematic diagram of the system under investigation. The shaded circle indicates a cylinder of infinite extension along the  $z$ -axis with diameter  $d$ .

The magnitude of the induced current, and thus the Lorentz force is linearly dependent on the fluid velocity (Müller and Bühler 2001). In the core region, where the velocity is higher than in the regions near the walls, the damping by the Lorentz force is stronger. This results in the counterbalancing effect between the damping force and the fluid flow, and thus the uniform velocity profile in the core region. It is also interesting to note that the

discrepancy between the quasi-2D and 3D velocity profile becomes smaller at higher Hartmann number, which supports the validity of the SM82 model for stronger magnetic field strength applications.

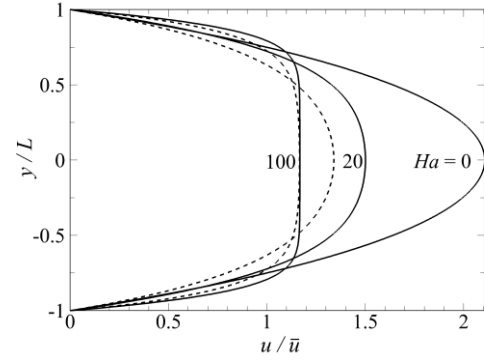


**Figure 2:** Velocity profiles at different Hartmann numbers, calculated from SM82 model (Pothérat 2007) (represented by the dashed lines) and analytical solution of a Shercliff flow (Shercliff 1953) at mid-plane ( $z = 0$ ) (represented by the solid lines). Velocity is normalized with the bulk flow velocity. Profile with  $Ha = 0$  represents analytical solution for normal hydrodynamic flow (Frank 1991).

Under the SM82 model the non-dimensional magnetohydrodynamic equations of continuity, momentum and energy reduce to

$$\nabla \cdot \mathbf{u} = 0, \quad (1)$$

$$\frac{\partial \mathbf{u}}{\partial t} = -(\mathbf{u} \cdot \nabla) \mathbf{u} - \nabla p + \frac{1}{Re_L} \nabla^2 \mathbf{u} + \frac{H}{Re_L} \left( \frac{1}{n} \mathbf{u}_0 - \mathbf{u} \right), \quad (2)$$

and

$$\frac{\partial \theta}{\partial t} + (\mathbf{u} \cdot \nabla) \theta = \frac{1}{Pe} \nabla^2 \theta, \quad (3)$$

respectively.  $\mathbf{u}$ ,  $p$  and  $\theta$  are the velocity, pressure and temperature fields, respectively, projected onto a plane orthogonal to the magnetic field,  $\nabla$  is the gradient operator and  $\mathbf{u}_0$  is the force vector field. The dimensionless parameters Reynolds number, Hartmann friction parameter and Peclet number are defined as  $Re_L = U_0 L / \nu$ ,  $H = (L/a)^2 n B a \sqrt{\sigma / \rho \nu}$  and  $Pe = U_0 L / k = Re_L Pr$ , where  $L$  is half duct width,  $U_0$  is peak inlet velocity,  $B$  is imposed magnetic field,  $a$  is out-of-plane duct depth,  $n$  is the number of Hartmann walls (in the present study,  $n = 2$ ),  $Pr$  is Prandtl number,  $\sigma$ ,  $\rho$ ,  $\nu$  and  $k$  are electrical conductivity, density, kinematic viscosity and thermal conductivity of the liquid metal, respectively. Here length is scaled by  $L$ , velocity by  $U_0$ , pressure by  $\rho U_0^2$ , time by  $L/U_0$  and temperature by the temperature difference between the bottom and top walls,  $\Delta \theta$ .

In the momentum equation, the force vector field  $\mathbf{u}_0$  is defined as  $\mathbf{u}_0 = \mathbf{j} \times \mathbf{e}_z = \nabla \psi_0 \times \mathbf{e}_z$ , where  $\mathbf{j}$  is the electric current density and  $\psi_0$  is the electrical potential. Under a high magnetic field condition, the equations governing continuity of electric current and incompressibility are linear, so they may be averaged to give  $\nabla \cdot \mathbf{j} = j_w$ ,

$\mathbf{j} = Ha(\mathbf{E} + \mathbf{u} \times \mathbf{e}_z)$  and  $\nabla \cdot \mathbf{u} = 0$ , where  $Ha$  is Hartmann number. Here  $j_w$  is the current density injected at one or both of the confining planes, and  $\mathbf{E}$  is a dimensionless electrical field. The  $z$ -averaged current can be expressed as the gradient of a scalar  $\psi_0$  satisfying a Poisson equation with the source term being  $j_w$  as  $\mathbf{j} = \nabla \psi_0$  and  $\nabla^2 \psi_0 = -j_w$ .

This Poisson equation is first solved for a source term at the current injection point that is a Dirac function located at  $O = (0, d)$ , i.e.  $\Phi(x, y) = j_w(x, y) = I\delta(x, y - d)$ , on a domain extending infinitely in streamwise direction and bounded by duct side-walls at  $y = 0$  and  $y = 2L$ . Then, the solution is shifted in the negative- $y$  direction at a distance of  $L$  in accordance with the global coordinate system (i.e. zero being at the centre of the duct in the vertical direction). Imposing Neumann condition at the boundaries due to insulating Shercliff walls, i.e.  $\partial \psi_0 / \partial z = 0$  at  $y = -L$  and  $y = L$  leads to

$$\psi_0(x, y) = \ln \frac{1/4\pi}{\cosh(\pi x/2L) - \cos(\pi(y_L - d)/2L)} + \ln \frac{1/4\pi}{\cosh(\pi x/2L) - \cos(\pi(y_L + d)/2L)}. \quad (4)$$

$I$  is the current amplitude which is non-dimensionalized as  $\hat{I} = ILU_0\sqrt{\rho\nu\sigma} = IR_{e_L}\sqrt{\rho\nu^3\sigma}$ . The force field is then given by

$$\mathbf{u}_0 = \nabla \psi_0 \times \mathbf{e}_z = \left\langle \frac{\partial \psi_0}{\partial x}, \frac{\partial \psi_0}{\partial y}, 0 \right\rangle \times \mathbf{e}_z. \quad (5)$$

The electric current is injected from the cylinder in pulses with various amplitude,  $I$ , and angular frequency,  $\omega_f = 2\pi f_f$ , where  $f_f$  is the forcing frequency. The pulse width  $\tau/T$  is fixed at  $\tau/T = 0.25$ , where  $T$  is the period of the current oscillation. The time-averaged Nusselt number is quantified by

$$Nu = \frac{1}{tL_w} \int_0^{t_w} \int_0^L Nu_w(x, t) dt dx, \quad (6)$$

where  $L_w$  is the length of the heated bottom wall. It is important to note that  $Nu_w(x, t)$  is scaled with the characteristic length  $L$ . To quantify the efficiency of the current injection on the heat transfer, the efficiency index is adopted (Hussam & Sheard 2013) and is defined as

$$\eta = \frac{HR}{PR} = \frac{Nu/Nu_0}{\Delta P/\Delta P_0}, \quad (7)$$

where  $HR$  and  $PR$  are the heat transfer enhancement ratio and pressure penalty ratio,  $Nu_0$  is the time-averaged Nusselt number of the heated region of the duct without any current injection, and  $\Delta P$  and  $\Delta P_0$  are the time-averaged pressure drop across the duct, with and without current injection, respectively.

### Solver validation

A high-order, in-house solver based on a spectral element method for spatial discretization is employed to

simulate the cases. In order to verify the solver, vorticity profiles of quasi-2D MHD duct obtained from the numerical computations are compared with the analytical solution, which is given by  $\xi = \partial v / \partial x - \partial u / \partial y = \sqrt{H} \sinh(\sqrt{H}y) / (\cosh(\sqrt{H}) - 1)$ ,

where  $\xi$  is vorticity. The exact solution for  $u(y)$  is given in Poth rat (2007). Figure 3(a) shows that the results from the numerical computations is in excellent agreement with the analytical solutions. Regression analysis of the data reveal relative standard errors (RSEs - which evaluates the residuals relative to the computed data) of 0.41%, 0.55% and 0.83% for  $H = 500$ , 1000 and 2000, respectively. Since the Shercliff layer thickness is inversely proportional to the square root of Hartmann number, i.e.  $\delta_s = a Ha^{-1/2}$  (Poth rat 2007), the increased RSE with increasing friction parameter is expected due to the demand for finer resolution at higher  $H$ . The present solver was further validated by comparing the critical Reynolds number at the onset of vortex shedding from experimental data of Frank, Barleon and M ller (2001) with the results from the present computations, as shown in Fig. 3(b). A good agreement with published data is found, which again supports the accuracy of the present solver. Further validation of the code can be found in Hussam *et al.* (2012).

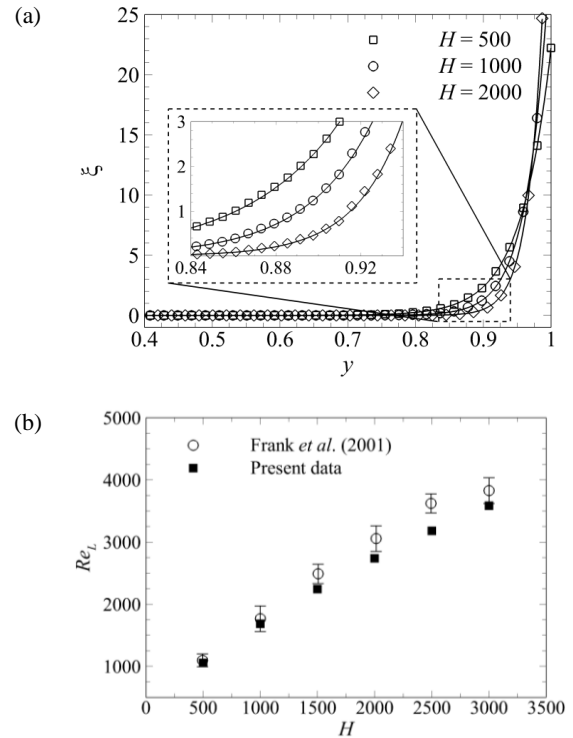


**Figure 3:** Vorticity profiles of fully developed quasi-2D duct flows in the vicinity of the side wall for  $Re = 3000$  and  $H$  as indicated. Symbols show results from present computations, while solid lines represent the analytical solution of SM82 model. (b) Critical  $Re_L$  at the onset of vortex shedding for  $\beta = 0.1$  and various magnetic field strength.

### Grid independence study

After constructing a mesh with elements distributed with increased density adjacent to side walls and cylinder and in the expected wake region, a grid independence study

was performed by varying the element polynomial degree from 4 to 11, while keeping the macro element distribution unchanged. The grid consists of four regions: two regions near the transverse walls, a core region, and a region in the vicinity of the cylinder. Small elements are distributed near the walls and the cylinder (as shown in Fig. 4) to resolve the expected high gradients in MHD flows and to capture the crucial characteristics of the boundary layer (e.g. boundary layer separation). The grid is also compressed in the horizontal direction towards the cylinder. The time-averaged Strouhal number ( $St$ ), total drag coefficient ( $C_D$ ), the integral of velocity magnitude throughout the domain ( $L_2$  norm) and Nusselt number ( $Nu$ ) were monitored, as they are known to be sensitive to the domain size and resolution.

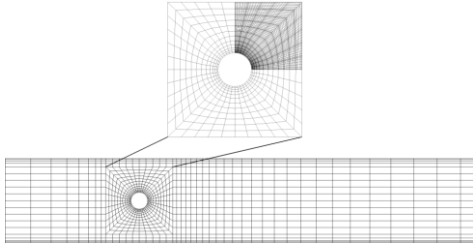


**Figure 4:** Macro-element distribution of the computational domain, and magnified mesh in the vicinity of the cylinder, with the upper right quadrant representing the spectral element distribution with  $N_p = 8$ . The mesh extends  $3.2L$  upstream and  $8L$  downstream.

Errors relative to the case with highest resolution,  $\varepsilon_p = |1 - P_N/P_{N=11}| \times 100\%$ , were defined as a monitor for each case, where  $P$  is the monitored parameter. A demanding MHD case with  $H = 500$ ,  $Re_L = 1500$ ,  $I = 60$ ,  $\omega_f = 4$  and  $\tau/T = 0.25$  was chosen for the test. The results are presented in Table 1, and show rapid convergence when the polynomial order increases. A mesh with polynomial degree 8 achieves at most a 0.9% error and is therefore used hereafter.

$N_p$	4	5	6	7	8	9	10
$\varepsilon_{St}$	0.405	0.390	0.271	0.262	0.188	0.170	0.088
$\varepsilon_{C_D}$	0.214	0.614	1.109	1.025	0.599	0.926	0.829
$\varepsilon_{L_2 \text{ norm}}$	0.030	0.110	0.181	0.176	0.104	0.110	0.045
$\varepsilon_{Nu}$	3.433	2.558	1.954	1.590	0.898	0.519	0.266

**Table 1:** Grid independence study at  $H = 500$ ,  $Re_L = 1500$ ,  $I = 60$ ,  $\omega_f = 4$  and  $\tau/T = 0.25$ .

## RESULTS AND DISCUSSION

### Heat Transfer Enhancement

This section reports the influence of magnetic field strength (quantified by friction parameter  $H$ ) and Reynolds number. Other parameters are fixed at  $I = 30$ ,  $\omega_f = 1.75$  and  $\tau/T = 0.25$ . The results are presented in Fig. 5 for  $200 \leq H \leq 2500$  and  $Re_L = 1500$  and  $3000$ . The figure shows that for a given Reynolds number, the enhancement in heat transfer due to the imposed current exhibit a non-monotonic relations with friction parameter. At low friction parameters (in the low- $H$  regime),  $HR$  increased

with increasing  $H$  and reach a peak, before decreased steadily with  $H$  (in the high- $H$  regime).

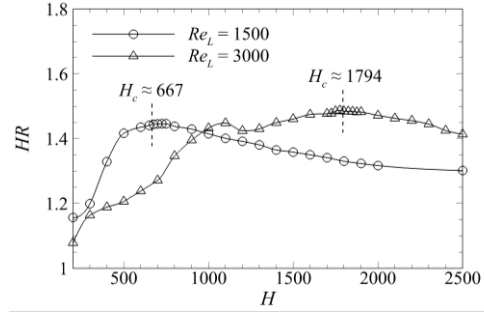


**Figure 5:** Heat transfer enhancement ratio plotted against friction parameter  $H$  for Reynolds number  $Re_L = 1500$  and  $Re_L = 3000$ . The dashed lines indicate critical friction parameter, above which the cylinder vortex shedding is completely suppressed.

This observation is attributed to the competition between the Lorentz force that is induced by the imposed current and the Hartmann damping force that is induced by the induced current. The former is represented by the positive forcing terms in the Navier–Stokes equation (i.e.  $H/nRe_L \mathbf{u}_0$  in equation (2) - a force that drives the vortex), while the latter is represented by the negative component in the forcing term in (i.e.  $-H/Re_L \mathbf{u}$ ). In the low- $H$  regime, the vortex-driving Lorentz force dominates over the damping force, which results in shed vortices maintain their vorticity for longer distance. There is a consistently strong interaction between the heated wall and the cylinder wake along the duct, visible in the vorticity field plot in Fig. 6(a).

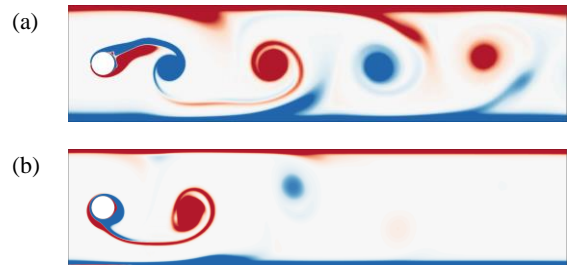


**Figure 6:** Instantaneous vorticity contour plots for  $Re_L = 1500$  and (a)  $H = 300$  and (b)  $H = 1500$ . Contour levels ranges between  $-2$  and  $2$ , with blue and red contours represent negative and positive vorticity, respectively

Consequently, the enhancement in the local Nusselt number is nearly uniform throughout the domain (as shown by the almost horizontal curve for  $H = 200$  in Fig. 7. In the high- $H$  regime, however, Hartmann damping dominates over the driving force. The strength of the shed vortices are relatively high in the near wake due to the strong interaction between the magnetic field and the imposed current forcing, but are damped almost immediately after they are shed (as indicated in the plot of vorticity contour in Fig. 6(b)). As a result, the strong wake-boundary layer interaction occurs only in the near wake region, which is reflected by the strong peak of local Nusselt number in the vicinity of the cylinder, followed by a rapid decline further downstream (as shown in Fig. 7 for friction parameters in the high- $H$  regime).

It is also interesting to note that the  $HR$  reaches its maximum value at a friction parameter close to the critical value  $H_c$  in which a transition between time-dependent and steady state flows occur in the base flows. The value of  $H$  was predicted by means of Stuart–Landau analysis, which was used to determine the growth or decay rates near the transition regime (further details concerning this analysis can be found in Hussam, Thompson and Sheard (2011)). Inspection of the time-averaged Nusselt number for the cases with the current injection at various friction parameters revealed two distinct peaks of different heights, the higher one being at  $H < H_c$  and the other one at  $H \approx H_c$  as shown in Fig. 8). The  $Nu$  for the base cases that correspond to the former peak is, however, higher than the latter, which results in the  $HR$  peaked at  $H \approx H_c$ . Figure 8 also shows that beyond the critical friction parameter, the Nusselt number reached an asymptote due to laminarization, and that the flow with higher  $Re_L$  reached a higher asymptote in the steady state regime.

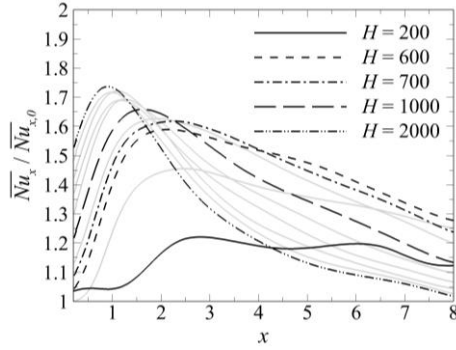


**Figure 7:** Normalized time-averaged local Nusselt number along the downstream of the heated wall for  $Re_L = 1500$  and  $H$  as indicated.

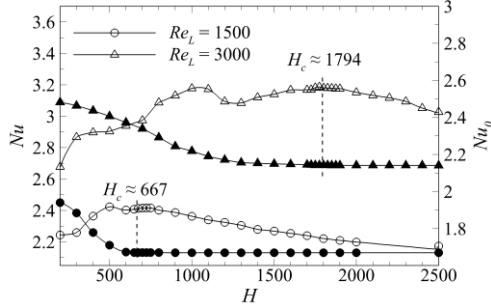


**Figure 8:** Time-averaged Nusselt number along the downstream of the heated wall, at various friction parameter. Circle and delta symbols represent  $Re_L = 1500$  and  $3000$ , respectively. Open symbols show cases with current injection (scaled on the primary vertical axis) and solid symbols show cases with the absence of current injection (scaled on the secondary vertical axis). The dashed lines indicate critical friction parameter.

#### Power and Efficiency Analysis

In this section, the characteristics of pumping power requirement (expressed in terms of pressure penalty ratio  $PR$ ), overall system efficiency resulting from the employment of current injection as a turbulence enhancer and the current injection power input are reported. The pressure penalty ratio  $PR$  in this study is the ratio of pressure drop across identical ducts with and without

current injection. Inspection of  $PR$  across all cases in this study (as shown in Fig. 9) revealed that the pressure drop induced by the imposed current injection is almost negligible, with the maximum pressure increment of 2.2% (i.e.  $PR_{max} = 1.022$ ). It has been shown previously that the pressure drop in an MHD duct flows is dominated by the Hartmann friction, in either empty duct (Barleon, Casal and Lenhart 1991) or in the presence of cylinder obstacle (Douset *et al.* 2008). Smolentsev, Morley, Wong and Abdou (2008) reported that the overall MHD pressure drop in the dual-coolant blanket module to be within the order of  $10^5 Pa$ .

It is also interesting to note that in some cases, the imposed current injection has a desirable effect by reducing the pressure drop with respect to the base cases, with a maximum reduction of 1% (i.e.  $PR_{min} = 0.99$ ). Since the  $PR$  is almost unity for all cases, it follows that that the system efficiency (quantified by the efficiency index  $\eta$  as in equation (7)) and the heat transfer enhancement ratio  $HR$  have a similar dependency on the varying parameters (as presented in Fig. 5).

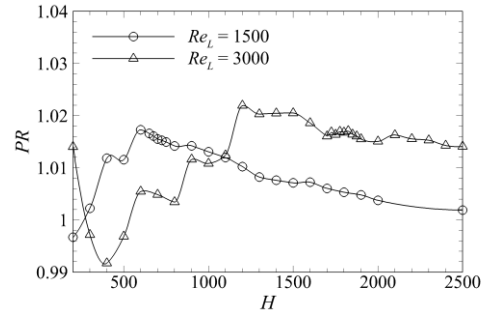


**Figure 9:** Pressure penalty ratio as a function of friction parameter for  $Re_L$  as indicated.

The power supply due to the current injection can be calculated as follows:

$$P(t) = I^2(t)R, \quad (8)$$

where  $R$  is resistance offered to the current flow. The time-averaged power is obtained by taking the root mean square (RMS) of injected current, i.e.

$$\bar{P} = I_{RMS}^2 R. \quad (9)$$

For a modified square wave,  $I_{RMS} = I_p \sqrt{D}$ , where  $I_p$  is the peak current amplitude, and  $D$  is the current pulse duty cycle, which is twice the pulse width, i.e.

$$D = 2 \frac{\tau}{T} \quad (10)$$

Hence, for  $\tau/T = 0.25$ ,

$$\bar{P} = 2 \frac{\tau}{T} I_p^2 R = \frac{I_p^2 R}{2}. \quad (11)$$

Equation (11) states that, for a given current pulse width, the current power input is proportional to the squared of the peak current amplitude. Since  $\hat{I} = iLU_0 \sqrt{\rho\nu\sigma} = iRe_L \sqrt{\rho\nu^3\sigma}$ , and taking the properties of low-melting eutectic alloy  $Ga^{68}In^{20}Sn^{12}$  at  $20^\circ C$ , i.e. density  $\rho = 6.3632 \times 10^3 \text{ kgm}^{-3}$ , electrical conductivity  $\sigma =$

$3.30737 \times 10^6 \Omega^{-1} \text{m}^{-1}$ , and kinematic viscosity  $\nu = 3.4809 \times 10^{-7} \text{m}^2 \text{s}^{-1}$  (Barleon, Mack and Stieglitz 1996), hence the dimensional current injection amplitude is given by  $\hat{I} \approx 2.98 \times 10^{-5} I Re_L$ . In the present investigation, the highest Reynolds number is  $Re_L = 3000$ , while the current injection amplitude was fixed at  $I = 30$ . Hence the maximum dimensional current is  $\hat{I} \approx 2.7$  Ampere, respectively. For the sake of comparison, this current supply is three orders of magnitude lower than that required to induce the confining magnetic fields for fusion blanket MHD research in the MEKKA experimental facility (Barleon *et al.* 1996).

## CONCLUSION

The present study has investigated the characteristics of MHD flow and heat transfer enhancement by means of wakes behind a cylinder, with a current injection as a mean to intensify the vortical structures. The results indicate a maximum Nusselt number improvement due to the current injection of about 50%, and is highly dependant on the imposed magnetic field strength. A non-monotonic relationships between the heat transfer enhancement ratio  $HR$  and the forcing frequency and magnetic field strength were observed.

An examination of the local Nusselt number variation along the duct revealed that the heat transfer enhancement is closely associated with the resulting wake dynamics and their interactions with the heated wall. In the absence of current injection, the vortex shedding is completely inhibited when the friction parameter is increased beyond the critical value, and the Nusselt number reached an asymptote due to laminarization.

The analysis of the pressure drop indicates that there was no significant additional pump power required to drive the flow in the presence of current injection. The imposed current injection in this study is easily realized in real applications.

## ACKNOWLEDGEMENTS

This research was supported by the Australian Research Council through Discovery Grants DP120100153 and DP150102920, a high-performance computing time allocations from the National Computational Infrastructure (NCI), which is supported by the Australian Government, and the Monash SunGRID. A. H. A. H. is supported by the Malaysia Ministry of Education and the Universiti Teknologi MARA, Malaysia.

## REFERENCES

BARLEON, L., V. CASAL and L. LENHART (1991), "MHD flow in liquid-metal-cooled blankets", *Fusion Eng. Des.*, **14**(3), 401-412.

BARLEON, L., K.J. MACK and R. STIEGLITZ (1996). The MEKKA-facility: A flexible tool to investigate MHD-flow phenomena, Forschungszentrum Karlsruhe.

BESKOK, A., M. RAISEE, B. CELIK, B. YAGIZ and M. CHERAGHI (2012), "Heat transfer enhancement in a straight channel via a rotationally oscillating adiabatic cylinder", *Int. J. Therm. Sci.*, **58**, 61-69.

CELIK, B., U. AKDAG, S. GUNES and A. BESKOK (2008), "Flow past an oscillating circular cylinder in a channel with an upstream splitter plate", *Phys. Fluids*, **20**(10), 103603.

CELIK, B., M. RAISEE and A. BESKOK (2010), "Heat transfer enhancement in a slot channel via a transversely oscillating adiabatic circular cylinder", *Int. J. Heat Mass Transfer*, **53**(4), 626-634.

DOUSSET, V. and A. POTHÉRAT (2008), "Numerical simulations of a cylinder wake under a strong axial magnetic field", *Phys. Fluids*, **20**(1), 017104.

FRANK, M., L. BARLEON and U. MÜLLER (2001), "Visual analysis of two-dimensional magnetohydrodynamics", *Phys. Fluids*, **13**(8), 2287.

FRANK, M.W. (1991). Viscous fluid flow, McGraw-Hill, New York.

FU, W.-S. and B.-H. TONG (2004), "Numerical investigation of heat transfer characteristics of the heated blocks in the channel with a transversely oscillating cylinder", *Int. J. Heat Mass Transfer*, **47**(2), 341-351.

HUSSAM, W.K. and G.J. SHEARD (2013), "Heat transfer in a high Hartmann number MHD duct flow with a circular cylinder placed near the heated side-wall", *Int. J. Heat Mass Transfer*, **67**, 944-954.

HUSSAM, W.K., M.C. THOMPSON and G.J. SHEARD (2011), "Dynamics and heat transfer in a quasi-two-dimensional MHD flow past a circular cylinder in a duct at high Hartmann number", *Int. J. Heat Mass Transfer*, **54**(5), 1091-1100.

HUSSAM, W.K., M.C. THOMPSON and G.J. SHEARD (2012), "Enhancing heat transfer in a high Hartmann number magnetohydrodynamic channel flow via torsional oscillation of a cylindrical obstacle", *Phys. Fluids*, **24**(11), 113601.

HUSSAM, W.K., M.C. THOMPSON and G.J. SHEARD (2012), "Optimal transient disturbances behind a circular cylinder in a quasi-two-dimensional magnetohydrodynamic duct flow", *Phys. Fluids*, **24**(2), 024105.

MÜLLER, U. and L. BÜHLER (2001). Magnetofluidynamics in Channels and Containers, Springer.

POTHÉRAT, A. (2007), "Quasi-two-dimensional perturbations in duct flows under transverse magnetic field", *Phys. Fluids*, **19**(7), 074104.

POTHÉRAT, A. and R. KLEIN (2014), "Why, how and when MHD turbulence at low becomes three-dimensional", *J. Fluid Mech.*, **761**, 168-205.

SHERCLIFF, J. (1953). Steady motion of conducting fluids in pipes under transverse magnetic fields. Mathematical Proceedings of the Cambridge Philosophical Society, Cambridge Univ Press.

SMOLENTSEV, S., N.B. MORLEY, C. WONG and M. ABDOU (2008), "MHD and heat transfer considerations for the US DCLL blanket for DEMO and ITER TBM", *Fusion Eng. Des.*, **83**(10), 1788-1791.

SOMMERIA, J. and R. MOREAU (1982), "Why, how, and when, MHD turbulence becomes two-dimensional", *J. Fluid Mech.*, **118**, 507-518.